



Exploring a link between the Middle Eocene Climatic Optimum and Neotethys continental arc flare-up

Annique van der Boon^{*1}, Klaudia F. Kuiper², Robin van der Ploeg¹, Margot J. Cramwinckel¹, Maryam Honarmand³, Appy Sluijs¹, Wout Krijgsman¹

5 **Corresponding author, present address: Geomagnetic Laboratory, Oliver Lodge Building, Department of Physics, Oxford Street, Liverpool, L69 7ZE, United Kingdom, AvanderBoon.work@gmail.com*

¹ *Department of Earth Sciences, Utrecht University, The Netherlands; Princetonlaan 8a, 3584 CB Utrecht, The Netherlands, R.vanderPloeg@uu.nl, M.J.Cramwinckel@uu.nl, A.Sluijs@uu.nl, W.Krijgsman@uu.nl*

10 ² *Dept. of Earth Sciences, Faculty of Science, Vrije Universiteit Amsterdam, De Boelelaan 1085, 1081 HV Amsterdam, The Netherlands, K.F.Kuiper@vu.nl*

³ *Department of Earth Sciences, Institute for Advanced Studies in Basic Sciences (IASBS), P.O. Box 45195-1159, Zanjan, Iran, M.Honarmand@iasbs.ac.ir*

15 **Abstract.** The Middle Eocene Climatic Optimum (MECO), a ~500 kyr episode of global warming that initiated at ~40.5 Ma, is postulated to be driven by a net increase in volcanic carbon input, but a direct source has not been identified. Here we show, based on new and previously published radiometric ages of volcanic rocks, that the interval spanning the MECO corresponds to a massive increase in continental arc volcanism in Iran and Azerbaijan. Ages of Eocene extrusive volcanic rocks in all volcanic provinces in Iran cluster around 40 Ma, very close to the peak warming phase of the MECO. Based on
20 the spatial extent and volume of the volcanic rocks as well as the carbonaceous lithology in which they are emplaced, we estimate the total amount of CO₂ that could have been released at this time corresponds to between 1500 and 11300 Pg carbon. This is compatible with the estimated carbon release during the MECO. Although the uncertainty in both individual ages, and the spread in the compilation of ages, is larger than the duration of the MECO, a flare-up in Neotethys subduction zone volcanism represents a plausible excess carbon source responsible for MECO warming.

25 1 Introduction

The MECO is characterized by surface and deep ocean warming, both of approximately 2-6°C. MECO warming initiated at ~40.5 Ma, culminating in a short peak warming phase at ~40.0 Ma and terminating at ~39.9 Ma with a comparatively rapid cooling (Bijl et al., 2010; Bohaty et al., 2009; Bohaty and Zachos, 2003; Boscolo Galazzo et al., 2014; Cramwinckel et al., 2018). The MECO is associated with a rise in atmospheric CO₂ concentrations (Bijl et al., 2010; Henehan et al., 2020),
30 extensive deep sea carbonate dissolution (Bohaty et al., 2009) and marine biotic change (Bijl et al., 2010; Cramwinckel et al., 2019; Edgar et al., 2013; Witkowski et al., 2012). The MECO inherently differs from the early Paleogene transient



warming events such as the Paleocene-Eocene Thermal Maximum (PETM; ~56 Ma) primarily in its longer duration (~500 kyr) of warming, precluding a sudden trigger but rather suggesting a continued driver (Bohaty and Zachos, 2003; Sluijs et al., 2013). Furthermore, unlike the PETM and similar transients, the MECO is not characterized by a negative $\delta^{13}\text{C}$ excursion of the exogenic carbon pool, ruling out the input of ^{13}C -depleted organic-sourced carbon as a driver, but suggesting a volcanic source (Bohaty and Zachos, 2003). Reconstructions and simulations of the carbon cycle indeed point to an imbalance in the long-term inorganic carbon cycle during the MECO (Sluijs et al., 2013), caused by enhanced volcanism and sustained by diminished continental silicate weathering (van der Ploeg et al., 2018). However, this scenario is quantitatively far from settled, partly because recent analyses based on foraminifer boron isotope ratios suggest that atmospheric CO_2 concentrations rose by significantly less than a doubling and did not rise substantially during the onset of the MECO (Henehan et al., 2020). In addition, a plausible source of excess volcanic CO_2 remains to be identified.

Here, we explore a volcanic arc flare-up in the Neotethys subduction zone as a potential source. Arc flare-ups can generate 80-90% of the total volume of igneous rocks in arc systems in periods of a few million years (Ducea and Barton, 2007). During the Eocene, a large flare-up took place in vast areas of present-day Iran (see Figure 1A) and these volcanic rocks show subduction-related geochemical signatures, representative of continental arc volcanism (Moghadam et al., 2015; Pang et al., 2013; Verdel et al., 2011). The main volcanic arc associated with the Neotethys subduction zone stretches from Bazman in southeast Iran towards Azerbaijan in the northwest, from where it continues westwards into Armenia, Georgia and Turkey (van der Boon et al., 2017). North of the volcanic arc, in the Peri-Tethys basin of Azerbaijan and Russia, thick bentonites and ash layers are found within middle Eocene marine sediments (Beniamovski et al., 2003; Seidov and Alizade, 1966).

Sahandi et al. (2014) produced a compilation of geological maps of Iran, which shows that more than half of the outcrop area of igneous rocks in Iran is of Eocene age (see Figure 1A). The total surface area that is covered by Eocene igneous rocks is almost 70.000 km² (including units mapped as Middle Eocene, Eocene-Oligocene, etc.). A causal relationship between peak volcanism in this region and the MECO has been suggested (Allen and Armstrong, 2008; Kargaranbafghi and Neubauer, 2018), but radio-isotopic age constraints to test this hypothesis are insufficient. To quantitatively assess whether volcanism in the Iran-Azerbaijan region could have been a contributor to global warming during the MECO, we present a compilation of new and previously published radiometric ages for volcanic rocks and estimate eruptive volumes of the flare-up in Iran to evaluate how much CO_2 could have been released during this event.

2 Dating the continental arc flare-up of the Neotethys subduction zone

2.1 New $^{40}\text{Ar}/^{39}\text{Ar}$ data

We analyzed 48 samples of Eocene volcanic rocks of the Azerbaijan-Bazman Arc in Iran and Azerbaijan. Lava flows of the Peshtasar formation were dated by Vincent et al. (2005) and van der Boon et al. (2017), but ages suffered from severe excess



argon. Here, we re-dated lava flows from the lower and middle part of the Peshtasar formation using new instrumentation to
65 check for potential age bias caused by hydrocarbon interferences in previous data. We further dated samples of two ash
layers in the Kura basin in Azerbaijan, as well as four volcanic rocks from the Talesh and western Alborz in Iran (see Figure
1B). Depending on the rock type, groundmass, plagioclase, sanidine, biotite and/or glass was measured (see Table 1). Thin
section analysis showed pervasive alteration of volcanic rocks, disqualifying many sampled units for radio-isotope dating
(see supplementary file S1 for a comparison of some thin sections). However, 8 samples showed no significant alteration and
70 were prepared for $^{40}\text{Ar}/^{39}\text{Ar}$ dating using standard mineral separation techniques including heavy liquid and magnetic
separation and handpicking. In general, fractions between 250-500 μm size were taken. For some minerals, both groundmass
or glass and plagioclase or biotite could be separated.

Samples were leached with diluted HNO_3 and/or HF. Samples were irradiated during resp. 12 and 18 hours in two
irradiations (VU101 in 2014 and VU107 in 2016) at the Oregon State University Triga CLICIT facility, together with Fish
75 Canyon Tuff sanidine as standard (FCs; 28.201 ± 0.023 Ma; Kuiper et al., 2008). After irradiation samples were loaded in
Cu-trays and run on a 10-collector Helix-MC mass spectrometer with an in-house built extraction with SEAS NP10, St172
and Ti sponge getters and a Lauda cooler run at -70°C , at the Vrije Universiteit Amsterdam. The used cup-configuration was
either ^{40}Ar on the H2 Faraday cup and 39-36 argon isotopes on compact discrete dynodes, or both ^{40}Ar and ^{39}Ar on
respectively H2 and H1 Faraday. Gain calibration was done by peakjumping CO_2 in dynamic mode on the different cups (see
80 Monster, 2016 for details). Samples were analyzed using step-heating experiments, while for the ash layers usually single or
a few grains were fused in one step and analyzed. Initial measurements were on single or a small number of grains, leading
in some samples to very low intensities of ^{40}Ar (3-4 times higher than blanks). In those cases, more grains were loaded in the
next experiment. Ages are calculated relative to the age of FCs reported in Kuiper et al. (2008; 28.201 ± 0.023 Ma) with
decay constants of Min et al. (2000).

85 Out of the 8 prepared samples, 7 gave results. Our new $^{40}\text{Ar}/^{39}\text{Ar}$ ages from igneous rocks and ash layers fall within a range
of ~ 36 -45 Ma (Figure 2A), with weighted mean ages per sample between 39.3-43.1 Ma (Figure 2B). Detailed results per
sample are described in supplementary file S4, and detailed results per experiment can be found in supplementary files S5-
S31. Multiple aliquots of the same samples were measured. Samples of lava flows were analyzed using step-heating
experiments, while for the ash layers usually single or a few grains were fused in one step and analyzed.

90 The integrated density distribution of these data reveals a peak at around 40.0 Ma. All compiled ages are shown together
with the scaled areal extent of mapped units of Sahandi et al. (2014) (see Figure 2C).

2.2 Compilation of literature data

We combined our newly acquired data with ~ 370 ages from 60 published studies, including K-Ar, Ar-Ar, U-Pb, Rb-Sr and
95 Re-Os ages (but mainly Ar-Ar and U-Pb; see supplementary file S2). Our age compilation aimed at pre-Quaternary rocks
and is incomplete with respect to Quaternary volcanic rocks in Iran. We then used a kernel density plot (Vermeesch, 2012) to



integrate all ages from 60-0 Ma, together with our newly acquired data. Ages and their 1σ uncertainties are used as input in the calculation of these distributions. Optimal bandwidth is calculated automatically, and we have set the bin width to 1 Myr. When studies did not report the significance level of their uncertainties, we assumed a 1σ uncertainty. Where possible, Ar-Ar ages were recalibrated to the standard of the Fish Canyon Tuff according to the Kuiper et al. (2008) calibration model. In some cases, original studies did not provide sufficient information for recalibration and then the original ages were used. All details of literature ages and associated references are added in supplementary files S2 and S3.

The compilation of $^{40}\text{Ar}/^{39}\text{Ar}$ ages from the literature, mostly from extrusive rocks (only 5 Ar-Ar ages are from intrusive rocks), yields a highly similar age density distribution to our dated samples (see Figure 3A), showing a peak at 39.7 Ma. Published U-Pb ages are typically obtained from zircons which provide less accuracy for eruption ages than $^{40}\text{Ar}/^{39}\text{Ar}$ ages from groundmass, plagioclase, sanidine or biotite (Simon et al., 2008), which is reflected in the greater width of the peaks from extrusive U-Pb ages (see Figure 3B). Combined, the Ar-Ar and U-Pb ages obtained from extrusive rocks record a 39.7 Ma peak, along with another sub-peak at 42.8 Ma (see Figure 3C).

3 Neotethys volcanism and the MECO

Considering that the Neotethys subduction zone has been active since the late Triassic (Arvin et al., 2007), our compilation shows a remarkable clustering of ages during the middle Eocene at ~40 Ma. Estimation of the areal extent of middle Eocene volcanic rocks is done using the shapefiles of Sahandi et al. (2014). For the Eocene, shapefiles are classified as 'Eocene', 'Eocene-Oligocene', 'Late Eocene-Oligocene', 'Middle Eocene', and 'Middle-Late Eocene'. We assumed that shapefiles specified as 'Eocene' had the same proportion of middle Eocene igneous rocks, and thus calculated an areal extent of 38223 km² of middle Eocene igneous rocks.

Our compilation indicates that many volcanic provinces in Iran were active simultaneously around 40 Ma (see Figure 2C), including the Azerbaijan-Bazman magmatic arc in the west, the Sabzevar zone in northeast Iran (Moghadam et al., 2015) and the Lut block in the east (Pang et al., 2013). Some of the largest volumes of middle Eocene volcanic rocks are located in the Talesh Mountains, where 4 out of 5 exposures with the largest areal extent are mapped (marked in white on Figure 1A). Almost three quarters of U-Pb ages (n=214) in Iran are derived from intrusive rocks (n=148). All ages of the intrusive rocks together reveal a peak at ~39.8 Ma (Figure 3D), indicating that the peak of middle Eocene extrusive volcanism is also close in time to peak intrusive activity.

It is thus clear that the MECO corresponds to a phase of intense volcanism in the studied area. However, the average error (1σ) of the literature-based ages from 20-60 Ma is 585 kyr, and thus exceeds the duration of the MECO (500 kyr). Furthermore, the exact ages of the peaks in volcanic activity in Figure 2 are sensitive to the number of data points included and are thus not particularly robust – the addition of a few new data points may shift the peaks by thousands of years.



4 Volcanic CO₂ emissions in Iran and the MECO

The surface area of Iran covered by middle Eocene extrusive volcanic rocks is almost 40.000 km² (Sahandi et al., 2014; Table 2). In the Alborz and Central Iran, middle Eocene extrusive volcanic formations are reported to be 3-9 kilometers thick
130 (e.g. Morley et al., 2009; Verdel et al., 2011). Extrapolating these thicknesses, this implies a total volume of extrusive middle Eocene volcanics between 1*10⁵ and 3.5*10⁵ km³ (see Table 2) that potentially produced significant amounts of CO₂. Due to the limited number of studies quantifying the relation between deposited volume of volcanic rocks and the emission of CO₂, we make a comparison with the Deccan traps, for which this relation has been calculated. The Deccan traps have an estimated eruptive volume of volcanic and volcanoclastic rocks of 1.3*10⁶ km³ (Jay and Widdowson, 2008), with an
135 associated emission 4.14*10¹⁷ mol CO₂ (Tobin et al., 2017). From different estimates of volume and related CO₂ emissions of Tobin et al. (2017), we obtain a linear relation of lava volume (in 10⁶ km³)/total CO₂ (in 10¹⁷ mol) ≈ 0.31 for the Deccan traps.

CO₂ degassing rates for continental arcs may be similar to (Marty and Tolstikhin, 1998), or larger than for continental flood basalts (McKenzie et al., 2016; Wignall et al., 2009). As a conservative starting point, we assume a similar volume versus
140 emission relationship as the Deccan traps, which implies a minimum estimate for CO₂ release from middle Eocene volcanism in Iran between 0.37*10¹⁷ and 1.10*10¹⁷ mol (see Table 2), which corresponds to 438-1315 Pg C. Moreover, the amount of CO₂ released during volcanic episodes has been shown to increase substantially if eruptions occur among carbonate-rich sediments (Lee et al., 2013; Lee and Lackey, 2015). For example, CO₂ released from carbonate sediments during the emplacement of the Emeishan large igneous province in the end-Guadalupian was estimated to be 3.6-8.6 times
145 higher than the amount of CO₂ released by volcanic outgassing alone (Ganino and Arndt, 2009). Indeed, the Eocene extrusive volcanism in Iran erupted through significant amounts of carbonate-rich rocks of Jurassic, Cretaceous, and Paleogene age (e.g. Berberian and King, 1981). As a result, carbon release associated with the production of volcanic rocks in Iran could be much larger, potentially ranging from 1578 to 11,308 Pg C (see Table 2). This range of CO₂ emissions is compatible with the carbon cycle imbalance that drives the MECO in simple carbon cycle simulations constrained by
150 available proxy data (roughly 2000-4000 Pg C; Henehan et al., 2020; Sluijs et al., 2013; van der Ploeg et al., 2018).

5 Future perspectives

There are several obstacles in solidifying the link between warming during the MECO and volcanism in the Neotethys subduction zone. First of all, continental arcs are generally active for (tens of) millions of years, while the MECO has a
155 duration of 500 kyr. Moreover, this duration is shorter than common uncertainties for radiometric ages in the Eocene, complicating the establishment of a causal relationship. This is important because a driver for the MECO requires excess CO₂ input only during the ~500 kyr spanning the MECO, and not during the time surrounding it (Sluijs et al., 2013). This is also supported by the drop in global ocean osmium isotope ratios, which is specifically associated with the MECO interval



(van der Ploeg et al., 2018). Secondly, Iran is a relatively understudied area compared to other (continental) arcs. As a result
160 of this, the amount of radiometric ages is low, with on average about 1 radiometric age for every several hundred km² of
outcrop.

Therefore, the relation in time between the MECO and Neotethys arc flare-up calls for the development of much better age
constraints of the volcanic deposits in Iran and this is certainly feasible. While most flare-ups have to be studied via their
intrusive roots, as the extrusive record is removed through erosion (Ducea and Barton, 2007; de Silva et al., 2015), the
165 extrusive record in Iran is extensive so that the ages can be mapped in high detail. Moreover, the respective roles of intrusive
and extrusive rocks can be assessed to estimate the amount of volatiles of the igneous rocks, and sedimentological studies
can provide minimum estimates on how much extrusive rock has been lost through erosion. This would help solve the
question if CO₂ input rates across from the Neotethys flare-up were truly excessive and caused a net addition of CO₂ during
the MECO.

170

6 Conclusions

We provide new Ar-Ar ages from volcanic rocks of the Azerbaijan-Bazman Arc in Iran and combine these with literature
data to show that a flare-up of continental arc volcanism in Iran peaked about 40 Ma ago, conspicuously close to the Middle
Eocene Climatic Optimum. We estimated volumes of middle Eocene volcanism in Iran to be between $1 \cdot 10^5$ and $3.5 \cdot 10^5$
175 km³. We compared the volume of middle Eocene volcanics in Iran to that of the Deccan traps and estimate that between 438
and 1315 Pg of carbon in the shape of CO₂ was released during deposition. Taking into account the fact that all volcanism
occurred in shallow marine basins and erupted in and through pre-existing carbonate-rich rocks, CO₂ release might have
been between 1578 and 11308 Pg. Although the flare-up must be dated much better to establish its chronological relation
with the MECO in more detail, we consider it a plausible major contributor to greenhouse warming during the MECO.

180

7 Supplementary materials

Examples of scans of thin sections are supplied in supplementary file S1. All details of literature ages and associated
references are added in supplementary files S2 and S3. A detailed description of Ar-Ar results per sample is provided in
supplementary file S4. Supplementary files S5-S31 show the results of the ⁴⁰Ar/³⁹Ar geochronology per experiment. S32
185 shows an extended version of the literature age plot of Figure 2C.

190

Author contributions: Fieldwork was undertaken by AvdB, MH and WK. AvdB, KFK and MH performed Ar-Ar dating.
Data analysis was performed by AvdB, KFK, RvdP, MJC and AS. All authors contributed to scientific discussions and were
involved in writing the manuscript.

Competing interests: The authors declare no competing interests.



Acknowledgements

195 This work was financially supported by Netherlands Organization for Scientific Research grant 865.10.011, awarded to WK,
and was carried out under the program of the Netherlands Earth System Science Centre, financially supported by the Dutch
Ministry of Education, Culture and Science. MLC and AS thank the Ammodo Foundation for funding unfettered research of
laureate AS. AS thanks the European Research Council for Consolidator Grant 771497 (SPANC). We thank Roel van Elsas
for help with Ar-Ar sample preparation.

200 References

- Agard, P., Omrani, J., Jolivet, L., Whitechurch, H., Vrielynck, B., Spakman, W., Monié, P., Meyer, B. and Wortel, R.:
Zagros orogeny: a subduction-dominated process, *Geol. Mag.*, 148(5–6), 692–725, doi:10.1017/S001675681100046X, 2011.
- Allen, M. B. and Armstrong, H. A.: Arabia – Eurasia collision and the forcing of mid-Cenozoic global cooling, *Palaeogeogr.*
205 *Palaeoclimatol. Palaeoecol.*, 265(1–2), 52–58, doi:10.1016/j.palaeo.2008.04.021, 2008.
- Arvin, M., Pan, Y., Dargahi, S., Malekizadeh, A. and Babaei, A.: Petrochemistry of the Siah-Kuh granitoid stock southwest
of Kerman, Iran: Implications for initiation of Neotethys subduction, *J. Asian Earth Sci.*, 30(3–4), 474–489,
doi:10.1016/j.jseaes.2007.01.001, 2007.
- 210 Beniamovski, V. N., Alekseev, A. S., Ovechkina, M. N. and Oberhänsli, H.: Middle to upper Eocene dysoxic-anoxic Kuma
Formation (northeast Peri-Tethys): Biostratigraphy and paleoenvironments, *Geol. Soc. Am. Spec. Pap.*, 369, 95–112, 2003.
- Berberian, M. and King, G. C. P.: Towards a paleogeography and tectonic evolution of Iran, *Can. J. Earth Sci.*, 18, 210–265,
215 1981.
- Bijl, P. K., Houben, A. J. P., Schouten, S., Bohaty, S. M., Sluijs, A., Reichert, G.-J., Damsté, J. S. S. and Brinkhuis, H.:
Transient Middle Eocene Atmospheric CO₂ and Temperature Variations, *Science*, 330, 819–821, 2010.
- 220 Bohaty, S. M. and Zachos, J. C.: Significant Southern Ocean warming event in the late middle Eocene, *Geology*, 31(11),
1017–1020, 2003.
- Bohaty, S. M., Zachos, J. C., Florindo, F. and Delaney, M. L.: Coupled greenhouse warming and deep-sea acidification in
the middle Eocene, *Paleoceanography*, 24, 1–16, doi:10.1029/2008PA001676, 2009.
- 225 van der Boon, A., Kuiper, K. F., Villa, G., Renema, W., Meijers, M. J. M., Langereis, C. G., Aliyeva, E. and Krijgsman, W.:



- Onset of Maikop sedimentation and cessation of Eocene arc volcanism in the Talysh Mountains, Azerbaijan, *Geol. Soc. London, Spec. Publ.*, 428, 145–169, doi:10.1144/sp428.3, 2017.
- 230 Boscolo Galazzo, F., Thomas, E., Pagani, M., Warren, C., Luciani, V. and Giusberti, L.: The middle Eocene climatic optimum (MECO): A multiproxy record of paleoceanographic changes in the southeast Atlantic (ODP Site 1263, Walvis Ridge), *Paleoceanography*, 29, 1–19, doi:10.1002/2014PA002670. Received, 2014.
- Cramwinckel, M. J., Huber, M., Kocken, I. J., Agnini, C., Bijl, P. K., Bohaty, S. M., Frieling, J., Goldner, A., Hilgen, F. J.,
235 Kip, E. L., Peterse, F., van der Ploeg, R., Röhl, U., Schouten, S. and Sluijs, A.: Synchronous tropical and polar temperature evolution in the Eocene, *Nature*, 559, 382–386, doi:10.1038/s41586-018-0272-2, 2018.
- Cramwinckel, M. J., van der Ploeg, R., Bijl, P. K., Peterse, F., Bohaty, S. M., Röhl, U., Schouten, S., Middelburg, J. J. and
240 Sluijs, A.: Harmful algae and export production collapse in the equatorial Atlantic during the zenith of Middle Eocene Climatic Optimum warmth, *Geology*, 47(3), 247–250, 2019.
- Ducea, M. N. and Barton, M. D.: Igniting flare-up events in Cordilleran arcs, *Geology*, 35(11), 1047–1050, doi:10.1130/G23898A.1, 2007.
- 245 Edgar, K. M., Bohaty, S. M., Gibbs, S. J., Sexton, P. F., Norris, R. D. and Wilson, P. A.: Symbiont “bleaching” in planktic foraminifera during the Middle Eocene Climatic Optimum, *Geology*, 41(1), 15–18, doi:10.1130/G33388.1, 2013.
- Ganino, C. and Arndt, N. T.: Climate changes caused by degassing of sediments during the emplacement of large igneous provinces, *Geology*, 37(4), 323–326, doi:10.1130/G25325A.1, 2009.
- 250 Henehan, M. J., Edgar, K. M., Foster, G. L., Penman, D. E., Hull, P. M., Greenop, R., Anagnostou, E. and Pearson, P. N.: Revisiting the Middle Eocene Climatic Optimum ‘Carbon Cycle Conundrum’ with new estimates of atmospheric pCO₂ from boron isotopes, *Paleoceanogr. Paleoclimatology*, doi:10.1029/2019PA003713, 2020.
- 255 Jay, A. E. and Widdowson, M.: Stratigraphy, structure and volcanology of the SE Deccan continental flood basalt province: implications for eruptive extent and volumes, *J. Geol. Soc. London.*, 165, 177–188, 2008.
- Kargarabafghi, F. and Neubauer, F.: Tectonic forcing to global cooling and aridification at the Eocene-Oligocene transition in the Iranian plateau, *Glob. Planet. Change*, 171, 248–254, doi:10.1016/j.gloplacha.2017.12.012, 2018.
- 260



- Kuiper, K. F., Deino, A., Hilgen, F. J., Krijgsman, W., Renne, P. R. and Wijbrans, J. R.: Synchronizing rock clocks of Earth history, *Science*, 320(5875), 500–4, doi:10.1126/science.1154339, 2008.
- 265 Lee, C.-T. A., Shen, B., Slotnick, B. S., Liao, K., Dickens, G. R., Yokoyama, Y., Lenardic, A., Dasgupta, R., Jellinek, M., Lackey, J. S., Schneider, T. and Tice, M. M.: Continental arc – island arc fluctuations, growth of crustal carbonates, and long-term climate change, *Geosphere*, 9(1), 21–36, doi:10.1130/GES00822.1, 2013.
- Lee, C. A. and Lackey, J. S.: Global Continental Arc Flare-ups and Their Relation to Long-Term Greenhouse Conditions, *Elements*, 11(2), 125–130, doi:10.2113/gselements.11.2.125, 2015.
- 270 Marty, B. and Tolstikhin, I. N.: CO₂ fluxes from mid-ocean ridges, arcs and plumes, *Chem. Geol.*, 145, 233–248, 1998.
- McKenzie, N. R., Horton, B. K., Loomis, S. E., Stockli, D. F., Planavsky, N. J. and Lee, C. A.: Continental arc volcanism as the principal driver of icehouse-greenhouse variability, *Science*, 352(6284), 444–447, doi:10.1126/science.aad5787, 2016.
- 275 Min, K., Mundil, R., Renne, P. R. and Ludwig, K. R.: A test for systematic errors in ⁴⁰Ar/³⁹Ar geochronology through comparison with U/Pb analysis of a 1.1-Ga rhyolite, *Geochim. Cosmochim. Acta*, 64(1), 73–98, 2000.
- Moghadam, H. S., Li, X.-H., Ling, X.-X., Santos, J. F., Stern, R. J., Li, Q.-L. and Ghorbani, G.: Eocene Kashmar granitoids (NE Iran): Petrogenetic constraints from U-Pb zircon geochronology and isotope geochemistry, *Lithos*, 216–217, 118–135, doi:10.1016/j.lithos.2014.12.012, 2015.
- 280 Monster, M.: Multi-method palaeointensity data of the geomagnetic field during the past 500 kyrs from European volcanoes, UU Dept. of Earth Sciences, Utrecht., 2016.
- 285 Morley, C. K., Kongwung, B., Julapour, A. A. A., Abdolghafourian, M., Hajian, M., Waples, D., Warren, J., Otterdoom, H., Srisuriyon, K. and Kazemi, H.: Structural development of a major late Cenozoic basin and transpressional belt in central Iran: The Central Basin in the Qom-Saveh area, *Geosphere*, 5(4), 325–362, doi:10.1130/GES00223.1, 2009.
- 290 Pang, K.-N., Chung, S.-L., Zarrinkoub, M. H., Khatib, M. M., Mohammadi, S. S., Chiu, H.-Y., Chu, C.-H., Lee, H.-Y. and Lo, C.-H.: Eocene–Oligocene post-collisional magmatism in the Lut–Sistan region, eastern Iran: Magma genesis and tectonic implications, *Lithos*, 180–181, 234–251, doi:10.1016/j.lithos.2013.05.009, 2013.
- van der Ploeg, R., Selby, D., Cramwinckel, M. J., Li, Y., Bohaty, S. M., Middelburg, J. J. and Sluijs, A.: Middle Eocene



- 295 greenhouse warming facilitated by diminished weathering feedback, *Nat. Commun.*, 9(1), 2877, doi:10.1038/s41467-018-05104-9, 2018.
- Sahandi, R., Soheili, M., Sadeghi, M., Delavar, T. and Jafari Rad, A.: Compiled geological map of Iran, scale 1:1.000.000, digitally published by the Geological Survey of Iran., 2014.
- 300 Seidov, A. G. and Alizade, K. A.: The formation and mineralogy of bentonites in Azerbaijan, *Clay Miner.*, 6, 157–166, 1966.
- de Silva, S. L., Riggs, N. R. and Barth, A. P.: Quickening the pulse: Fractal tempos in continental arc magmatism, *Elements*, 305 11(2), 113–118, doi:10.2113/gselements.11.2.113, 2015.
- Simon, J. I., Renne, P. R. and Mundil, R.: Implications of pre-eruptive magmatic histories of zircons for U-Pb geochronology of silicic extrusions, *Earth Planet. Sci. Lett.*, 266(1–2), 182–194, doi:10.1016/j.epsl.2007.11.014, 2008.
- 310 Sluijs, A., Zeebe, R. E., Bijl, P. K. and Bohaty, S. M.: A middle Eocene carbon cycle conundrum, *Nat. Geosci.*, 6(June 2013), 429–434, doi:10.1038/ngeo1807, 2013.
- Tobin, T. S., Bitz, C. M. and Archer, D.: Modeling climatic effects of carbon dioxide emissions from Deccan Traps volcanic eruptions around the Cretaceous – Paleogene boundary, *Palaeogeogr. Palaeoclimatol. Palaeoecol.*, 478, 139–148, 315 doi:10.1016/j.palaeo.2016.05.028, 2017.
- Verdel, C., Wernicke, B. P., Hassanzadeh, J. and Guest, B.: A Paleogene extensional arc flare-up in Iran, *Tectonics*, 30, doi:10.1029/2010TC002809, 2011.
- 320 Vermeesch, P.: On the visualisation of detrital age distributions, *Chem. Geol.*, 312–313, 190–194, doi:10.1016/j.chemgeo.2012.04.021, 2012.
- Vincent, S. J., Allen, M. B., Ismail-Zadeh, A. D., Flecker, R., Foland, K. A. and Simmons, M. D.: Insights from the Talysh of Azerbaijan into the Paleogene evolution of the South Caspian region, *Geol. Soc. Am. Bull.*, 117(11), 1513–1533, 325 doi:10.1130/B25690.1, 2005.
- Wignall, P. B., Sun, Y., Bond, D. P. G., Izon, G., Newton, R. J., Védérine, S., Widdowson, M., Ali, J. R., Lai, X., Jiang, H., Cope, H. and Bottrell, S. H.: Volcanism, Mass Extinction, and Carbon Isotope Fluctuations in the Middle Permian of China,



Science, 324, 1179–1182, doi:10.1126/science.1171956, 2009.

330

Witkowski, J., Bohaty, S. M., McCartney, K. and Harwood, D. M.: Enhanced siliceous plankton productivity in response to middle Eocene warming at Southern Ocean ODP Sites 748 and 749, *Palaeogeogr. Palaeoclimatol. Palaeoecol.*, 326–328, 78–94, doi:10.1016/j.palaeo.2012.02.006, 2012.

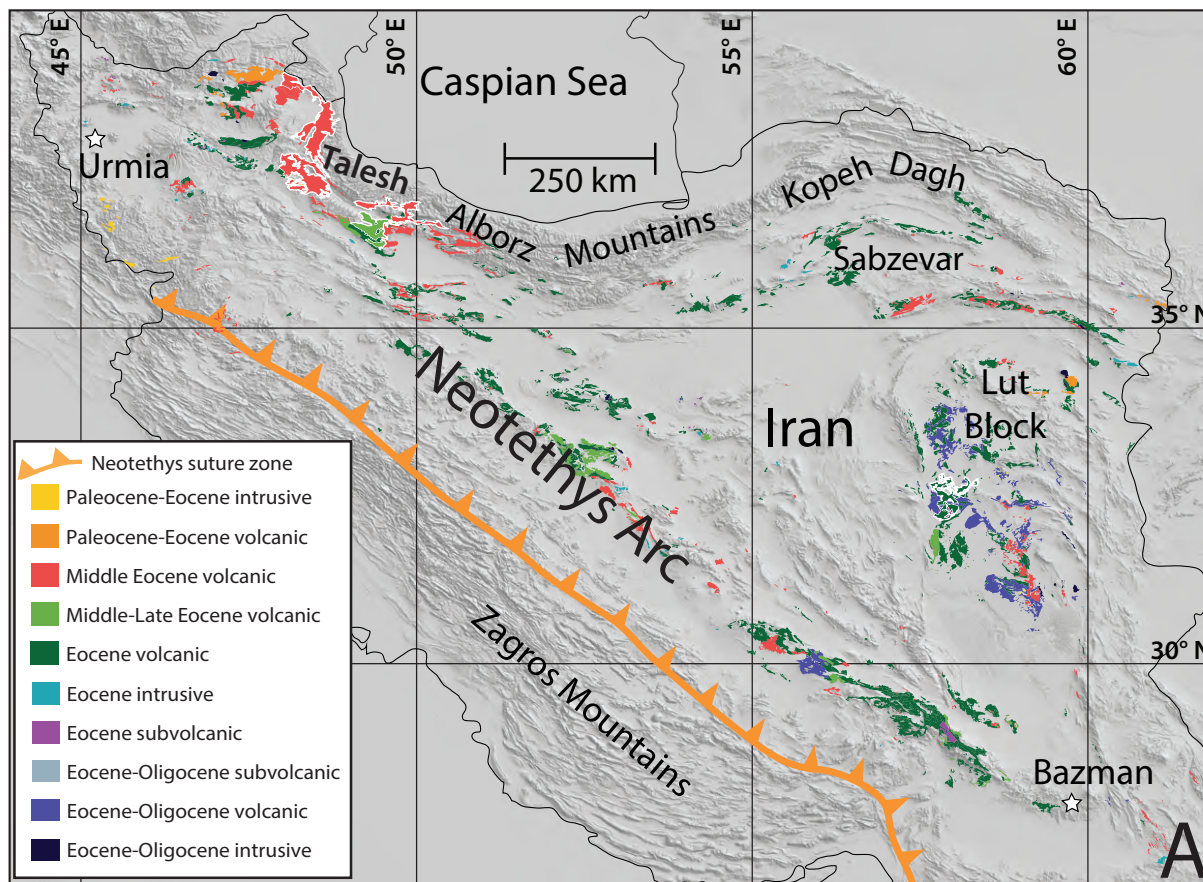


Figure 1:
A. Map showing the outcrop of Eocene volcanic rocks in Iran (modified after Agard et al., (2011) and shapefiles of Sahandi et al., (2014)). The five largest areas are shown with white outlines.
B. Sample locations of newly acquired $^{40}\text{Ar}/^{39}\text{Ar}$ ages.

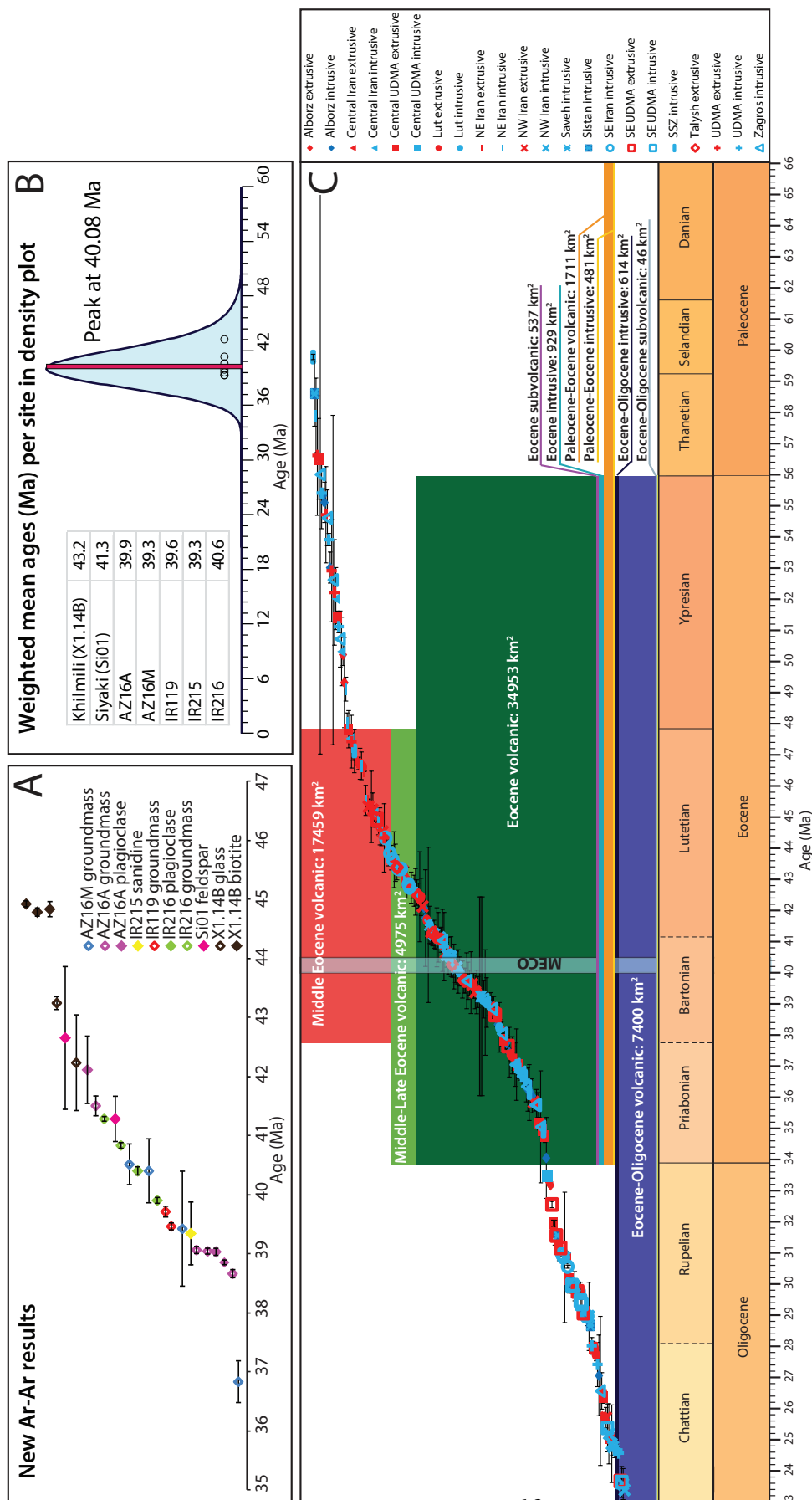


Figure 2:

A. ⁴⁰Ar/³⁹Ar dates of rocks from northwest Iran, south Azerbaijan and the Kura basin with uncertainties (1σ).

B. Kernel density plot in blue (Vermeesch, 2012) of combined ⁴⁰Ar/³⁹Ar ages. The duration and timing of the MECO event is indicated by the pink band.

C. Timescale (created with TSCreator) with scaled eruptive areas (from Sahandi et al., 2014), color legend for areas is the same as in figure 1A. Also plotted are radiometric ages from literature with associated 1σ errors, sorted by age, Y-axis is arbitrary unit. Red markers represent extrusive ages, blue markers represent intrusive ages.

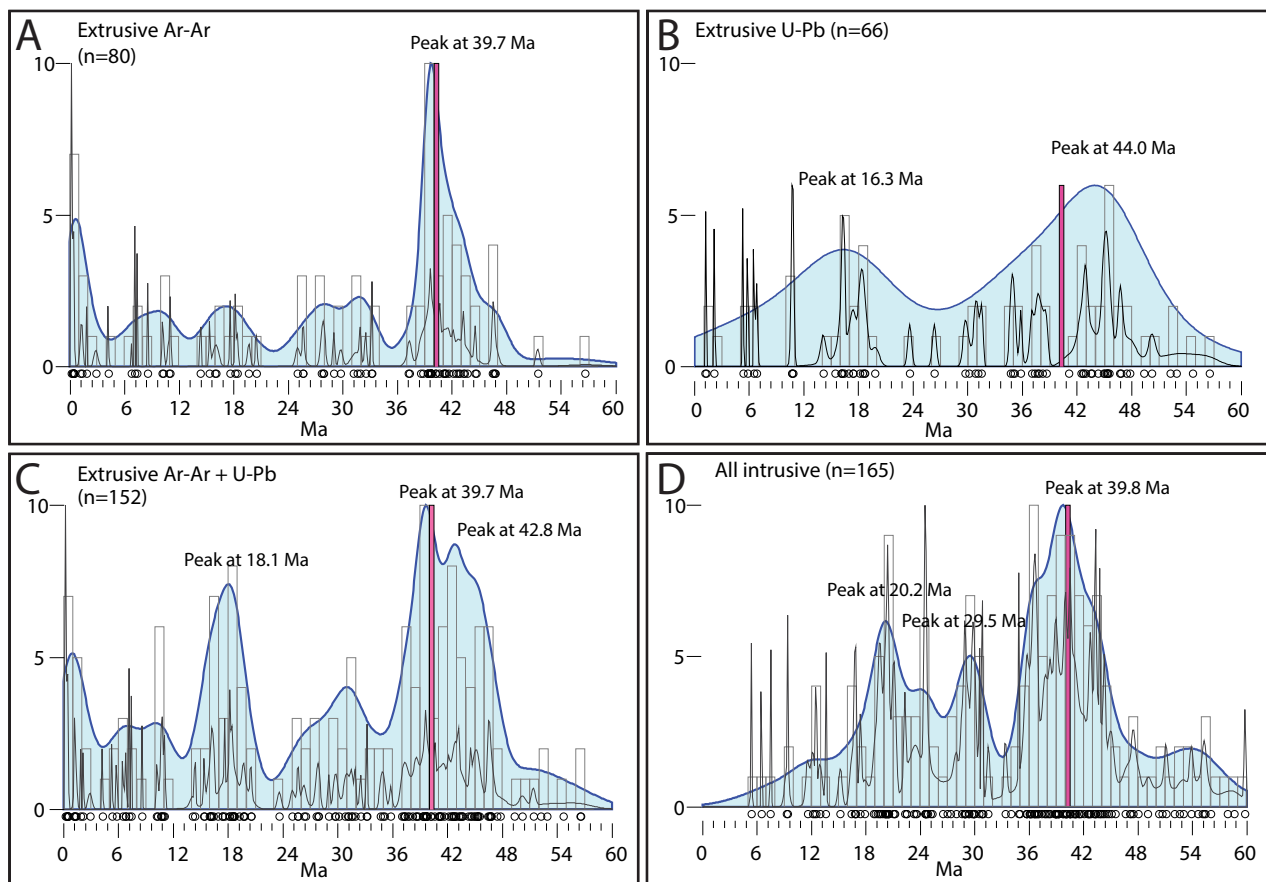


Figure 3:

Radio-isotope ages from 0-60 Ma, compiled from literature, combined with our newly obtained ages. Black thin line represents the probability density plot (PDP), blue filled line represents the kernel density estimate (KDE), boxes represent histograms (numbers on Y-axis). The timing and duration of the MECO is indicated by the pink box.

- A. $^{40}\text{Ar}/^{39}\text{Ar}$ ages from literature combined with newly obtained ages for extrusive rocks only.
- B. U-Pb ages from literature for extrusive rocks only.
- C. $^{40}\text{Ar}/^{39}\text{Ar}$ data and U-Pb data from extrusive rocks only.
- D. Combined ages from literature for intrusive rocks only.



Region	Section	Formation	Type	Sample	Lat	Long	Areal extent on shapefile (km ²)	Mineral	Excel file	Age plateau	Error (2σ)
Kura basin (Azerbaijan)	Khilmili	Koun	Ash	X1.14B	40.68640	48.87632	N/A	glass	VU101C-A4a	42.23	1.62
									VU101B-A4e	43.24	0.20
								biotite	VU101B-A8a	44.83	0.25
									VU101B-A8b	44.78	0.13
									VU101B-A8e	44.92	0.11
Kura basin (Azerbaijan)	Siyaki	Koun	Ash	Si01	40.54582	49.25776	N/A	feldspar	VU101B-A7a	42.65	2.43
									VU101B-A7e	41.28	0.78
Talysh (Azerbaijan)		Peshtasar	Basalt	AZ16A	38.86672	48.05018	N/A	groundmass	VU101B-A1c	41.50	0.35
									VU101B-A1da	39.06	0.12
									VU101B-A1db	39.04	0.11
									VU101B-A1f	38.66	0.16
								plagioclase	VU101B-A3c	42.11	1.12
									VU101B-A3da	39.03	0.06
									VU101B-A3db	38.85	0.10
Talysh (Azerbaijan)		Peshtasar	Basalt	AZ16M	38.90105	48.09660	N/A	groundmass	VU101B-A2c	40.51	0.68
									VU101B-A2da	36.83	0.69
									VU101B-A2db	39.42	1.95
									VU101B-A2f	40.40	1.06
									VU101B-A2g	40.40	1.06
Talesh (Iran)		Karaj	Trachyte	IR119	38.62625	47.77411	168	groundmass	VU107-A2_1	39.71	0.09
									VU107-A2_2	39.46	0.12
Talesh (Iran)		Karaj	Trachyandesite	IR215	38.42648	47.95920	406	feldspar	VU107-A4_1	39.34	1.08
Talesh (Iran)		Karaj	Tracyandesite	IR216	38.40969	47.98619	406	plagioclase	VU107-A5_1	40.40	0.13
									VU107-A5_2	39.90	0.11
								groundmass	VU107-A6_1	41.28	0.10
									VU107-A6_2	40.83	0.11
Western Alborz (Iran)		Karaj	Trachybasalt	IR22	36.48612	48.98974	281	groundmass	VU107-A1_1	35.98	1.11
									VU107-A1_2	51.64	1.26

Table 1:

Details of samples that were prepared for ⁴⁰Ar/³⁹Ar geochronology.

Area (km ²)	Thickness (km)	Volume (km ³)		vol Iran/Deccan	CO ₂ Iran (mol)	C (pg)	CO ₂ limestone multiplier	CO ₂ with 1st (pg)	C with 1st (pg)
38223	3	114669	1.15.E+05	0.09	3.65E+16	438	3.6	5786	1578
		114669	1.15.E+05	0.09	3.65E+16	438	8.6	13821	3769
	6	229338	2.29.E+05	0.18	7.30E+16	877	6.1	19607	5347
	9	344007	3.44.E+05	0.26	1.10E+17	1315	3.6	17357	4734
		344007	3.44.E+05	0.26	1.10E+17	1315	8.6	41464	11308

Table 2:

Calculated amounts of CO₂ released for different volume estimates of (middle) Eocene volcanism in Iran.